

Automatic Measurement of Subregional Vertebral Bone Mineral Density via Deep Learning of Quantitative Computed Tomography Images

Chentian Li^{1,2,3,#}, Chi Ma^{1,2,#}, Xianglong Zhuo^{4,#}, Wei Wang¹, Li Li^{2,4}, Wing-Yuk Ip², Bing Li⁴, Tao Li⁴, Songjian Li³, Feng Zhu^{1,2,*} and William W. Lu^{1,2,5,*}

¹Department of Orthopaedics, & Department of Radiology, the University of Hong Kong-Shenzhen Hospital, Shenzhen, Guangdong, P.R. China

²Department of Orthopaedics & Traumatology, Li Ka Shing Faculty of Medicine, The University of Hong Kong, Hong Kong SAR, P.R. China

³Department of Orthopaedics, Zhujiang Hospital, Southern Medical University, Guangzhou, Guangdong, P.R. China

⁴Department of Orthopaedics, & Department of Radiology, Liuzhou Worker's Hospital, Guangxi Medical University, Liuzhou, Guangxi, P.R. China

⁵Center for Human Tissues and Organs Degeneration, Shenzhen Institutes of Advanced 5 Technology, Chinese Academy of Science, Shenzhen, Guangdong, P.R. China

Abstract: *Background:* Measurement of subregional Bone Mineral Density (BMD) of the vertebral body has been shown to hold a critical role in osteoporotic fracture risk analysis. The reproducibility and precision of the measurement rely highly on the vertebral body region of interest segmentation accuracy, which requires expert-level experience in medical image preprocessing and is time-consuming work. The establishment of a reliable automatic method could enhance the efficiency and precision of these measurements in clinical practice.

Purpose: To develop and validate a deep learning-based segmentation approach for subregional vertebral BMD measurement with quantitative CT scans.

Materials and Methods: Quantitative CT images from 115 subjects (62 women and 53 men with a mean age of 66.4 ± 13.4 years) were retrospectively collected. A deep learning-based segmentation pipeline was trained on a total of 403 manual segmented lumbar vertebral bodies. The performance was evaluated by its accuracy, Dice Score, and Intersection over Union (IoU) score. A scan-rescan test was performed to evaluate the subregional BMD measurement reliability and reproducibility by analyzing the intraclass correlation coefficient and Bland-Altman analysis.

Results: This automatic approach achieved high segmentation performance for the entire vertebral body segmentation (accuracy 0.98 ± 0.02, dice coefficient 0.92 ± 0.06, and IoU 0.87 ± 0.09), cortical bone segmentation (accuracy 0.95 ± 0.02, dice coefficient 0.92 ± 0.03, and IoU 0.85 ± 0.05), and endplate segmentation (accuracy 0.89 ± 0.05 and Dice coefficient 0.75 ± 0.09, IoU 0.61 ± 0.12). The scan-rescan test further showed the automatic measurement is highly reproducible ($r = 0.96$, limit of agreement [LoA] = -20.4~17.9 mg/cm³ for entire region; $r = 0.95$, LoA = -39.5~33.3 mg/cm³ for cortical region; $r = 0.89$, LoA = -23.4~20.9 mg/cm³ for cancellous region; $r = 0.82$, LoA = -44.9~58.9 mg/cm³ for superior endplate; $r = 0.63$, LoA = -81.6~106.5 mg/cm³, respectively).

Conclusion: The deep learning-based approach is feasible for vertebral body subregions segmentation, which ensures the precision and reproducibility of BMD measurement. The cortical and cancellous BMD can be separately measured by the deep learning-based approach, providing an automatic and reliable framework for the investigation of subregional osteoporosis changes with Quantitative Computed Tomography (QCT) spine scans.

Keywords: Bone mineral density, Spine imaging, Deep learning, Atlas-based segmentation, Quantitative computed tomography.

1. INTRODUCTION

Identification of the vertebral body region of interest and the standardization of imaging analysis protocols with automatic approaches are important for the

improvement of bone mineral density (BMD) measurement precision for osteoporosis assessment [1-3]. Conducting the analysis steps automatically could standardize the measurement and reduce interobserver errors from manual manipulation. For computer-assisted spine image analysis, most of the previous studies addressed the entire vertebrae segmentation and achieved high accuracy on the fully automatic segmentation tasks [4].

*Address correspondence to this author at the Department of Orthopaedics, University of Hong Kong-Shenzhen Hospital, Shenzhen, Guangdong, P.R. China; Tel: +86-13688815442; E-mail: aaronzhu@hku.hk; wwlu@hku.hk

#These authors contributed equally to this work.

However, the task for vertebral osteoporosis assessment needs more mechanisms than solely the overall vertebral region segmentation. Since the cortical bone, the bony layer of endplates, and the cancellous bone have unique structural designs, the different subregions of the vertebral body have different fracture resistance capacity [5-7]. The accurate segmentation of those structures as separate compartments is crucial for the localized osteoporosis changes assessment and finite-element modeling [8, 9].

To date, the previously reported automatic segmentation solutions were only concerned with separating the entire vertebral region from other tissues. The automatic strategy for vertebra subregions (cortical bone, cancellous bone, and the bony layer of endplates) segmentation is rarely discussed [10]. Besides, since the clinical CT images are usually in low spatial resolutions, it makes the manual segmentation of vertebral subregions more challenging [9]. To achieve better performance on cortical bone and trabecular bone segmentation, the image analysis techniques, including image deblurring [11, 12] and cortical bone thickness estimation [13, 14] were proposed. However, a thoroughly designed automatic approach for vertebral subregions segmentation has not yet been developed for subregional vertebral BMD measurement using quantitative computed tomography (QCT).

In this study, we aimed to design an automatic pipeline for subregional vertebral BMD measurement based on a deep learning framework with a coarse-to-fine-grained attention strategy. The newly developed pipeline adopted hybrid strategies from state-of-the-art methods and was further optimized for vertebra subregions segmentation in QCT images. Furthermore, the reproducibility and precision of subregional BMD measurements based on this pipeline were validated.

2. MATERIALS AND METHODS

2.1. Data Selection and Study Design

The spine quantitative CT images were retrospectively reviewed after full institutional review board approval. Due to the retrospective nature of the study, the need for individual patient consent was waived. Patients of 20 years or older were selected. To generalize the application scenario, subjects with both healthy spines and those with vertebral body fractures were collected. In total, 57 subjects (24 women and 33 men with a mean age of 62.1 ± 15.4 years) with no

finding of vertebral body fracture, and 58 subjects (38 women and 20 men with a mean age of 70.7 ± 9.5 years) with vertebral body fracture prevalence were collected. To measure the volumetric bone mineral density in the thoracolumbar vertebrae, the T11~L5 spine level was chosen. In each scan, vertebrae with compression fracture or high deformation were excluded. A total of 403 vertebrae were included in this study.

2.2. QCT Acquisition

All images were obtained using the Siemens SOMATOM Definition Flash CT Scanner (Siemens, Germany). The scans were performed at 120 kV and automatic tube current mode, with 1.0 mm slice thickness and a field of view of 200 mm at the lumbar spine region. The images were routinely reconstructed with a reconstruction increment of 0.7 mm and B30s kernel, leading to an in-plane resolution of 0.4 mm and a z-axis resolution of 0.7 mm.

2.3. Manual Vertebral Body Segmentation

All the vertebral bodies were manually segmented to create the segmentation ground truth. The Fast GrowCut-based segmentation was performed for each CT image with Slicer v4.8.1(Kitware) [15]. The cortical and cancellous bone regions were separated using global threshold-based segmentation with manual removal of mislabeled regions. Then, the bony layer of the endplate regions and the cortical wall were manually separated.

2.4. Vertebral Body Atlas Generation for Atlas-Based Segmentation

A total of 30 healthy L1 and L2 lumbar vertebral body mask images from 15 young individuals (8 women and 7 men with a mean age of 29 ± 6.1 years) were manually segmented. The volume mask datasets of the vertebral body were loaded and reconstructed into 3D polygon models using ShapeWorks Studio [16]. In brief, the smoothing step was performed to reduce model complexity. Then, the optimization was performed to build the particle correspondence shape model. The number of corresponding particles was set to 10 and the relative weighting was set to 1.00 in the optimization step. Finally, the mean vertebral body shape model was generated and converted into volume data as a standard vertebral body shape image. To simulate the cortical and cancellous bone regions, the 1.5 mm distance inner region of the vertebral body contour was defined as the cortical bone region and labeled with a different value.

2.4. Segmentation Pipeline with a Coarse-To-Fine Strategy

A four-step coarse-to-fine strategy was proposed to segment the vertebral body subregions.

2.4.1. Preprocessing: Vertebral Body Location

Before vertebral body segmentation, the interested segmental level was selected by manually labeling the centroid region of the vertebral body in Slicer v4.8.1 [15]. Then, a $64 \times 64 \times 64$ mm bounding box was used to crop the image based on the labeled vertebral body

centroid. Finally, the cropped image patch was resized to $128 \times 128 \times 128$ voxel size for analysis.

2.4.2. Coarse-Grained: Vertebral Body Segmentation

An iterative convolutional neural network approach was adopted for single vertebral body segmentation [17]. In brief, a U-net like the fully convolutional neural network architecture was created to detect the vertebral body region from the cropped image patches one by one. The regions that had been segmented

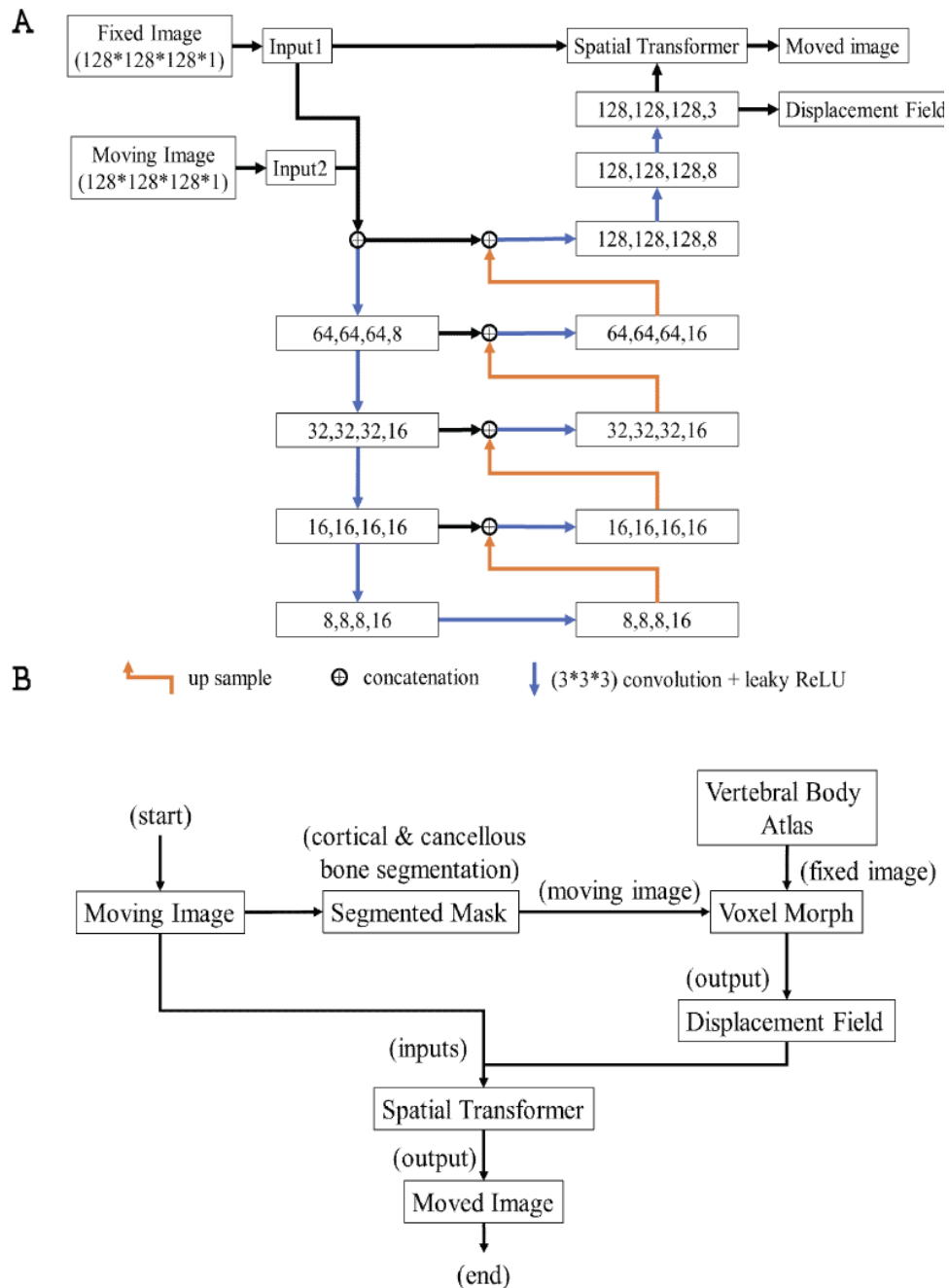


Figure 1: Optimized Voxel Morph model architecture (A) and atlas-based deformable registration strategy (B).

from the previous patch were recorded and ignored in the next patch.

2.4.3. Median-Grained: Cortical Bone Region Segmentation

We adopted a multi-scale Otsu threshold method [18] for the cortical region segmentation. In brief, the original image was filtered by the Gaussian filter with multi-sized sigma kernels (sigma = 0, 1, 2..., 9). Then, the Otsu threshold was performed on each filtered image and the binary masks were summed up as a fusion image. The region with a value above 5 was defined as the cortical region.

2.4.4. Fine-Grained: Atlas-Based Endplates Segmentation

An atlas-based segmentation approach was adopted for endplates segmentation. For the atlas-based segmentation, images were deformably registered to a standard atlas, then a preset segmentation mask was overlapped on the registered image to find the region of interest.

In brief, the image registration was performed by two steps: (1) "rigid alignment" and (2) "non-rigid

registration." An automatic rigid registration was performed for each vertebral body image to make sure each vertebral body were rigidly registered to the vertebral body atlas using the SimpleElastix v.0.1 [19]. After rigid registration, the VoxelMorph framework based on unsupervised deep learning was applied for fast deformable registration [20] (Figure 1.A). After the deep learning model training, the spatial displacement field was predicted from the VoxelMorph model based on the pair of vertebral body atlas and cortical segmented images for deformable registration (Figure 1.B).

To segment the endplate regions, the atlas of endplate regions was adaptively generated based on a morphological transform method. In brief, the registered cortical region mask was filtered by a grayscale morphological opening operation with a disk-like structure element with a radius of 8 voxels in scikit-image v.0.17 (open source). Then, a similarity score was generated by voxel-wise multiply of the filtered image and the cortical image. Voxels with a similarity score above 0.05 were considered as the endplate region (Figure 2). Finally, a VoxelMorph-based deformable registration was performed using the

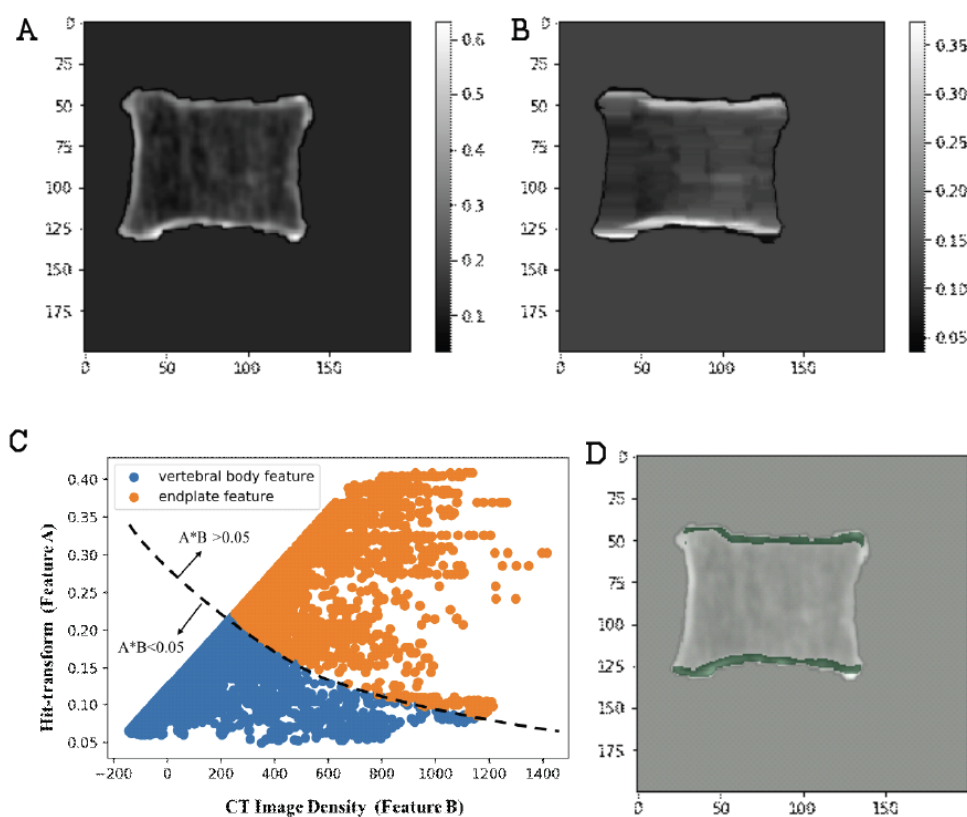


Figure 2: Voxel-wise scatters plot of morphological feature and density feature values for endplate thresholding. (A. Original registered image, B. Morphological 'hit-transformed' image, C. Voxel-wise relationship between density and hit-transform features. The endplate features were usually above the dashed curve; D. Endplate segmentation results colored in green)

endplate mask atlas as a moving image and the cortical mask image of the original CT image as the target image. After deformable registration, the mask would cover the endplate regions in the original CT image (Figure 3).

2.5. Deep Learning Models Training

To implement the methods mentioned above, a home-made program was built with Python 3.5 (open source; Python Software Foundation, Wilmington, DE). Scikit-image and NumPy library were used for the implementation. Keras v2.1.2 with Tensor Flow-GPU v1.3 was used for deep learning. The experiments were performed in Intel Core i7 CPU and NVIDIA GTX 1080Ti GPU (Nvidia, Santa Clara, CA) and 16GB RAM with CUDA 8.0 (Nvidia) in the Ubuntu v16.04 operating system (Canonical, London, England).

For iterative U-net model training, a Tversky loss [21] was with alpha 0.7 and beta 0.5. For VoxelMorph model training, the cortical bone segmentation mask datasets were randomly paired as the moving and fixed image for unsupervised Voxel Morph model training. The training loss was defined as the combination of appearance similarity loss [the mean square error

(MSE) loss was used] and smooth displacement loss weighted by 1 and 0.1, separately. The details of the definition of similarity and displacement loss can be found in the original paper by Balakrishnan *et al.* [20].

In all models, the ‘Adam’ optimization method was used for the model parameters training. To evaluate the training performance, 80% of the datasets were randomly chosen as a training dataset and 20% as a validation dataset. The iterative U-net model was trained by 150 epochs with a batch size of 4 datasets. The Voxel model was trained by 50 iterations per epoch for 1000 epochs with a batch size of 8 pairs.

2.6. Automatic Segmentation Performance Assessment

2.6.1. Data Selection

An extra dataset with 8 vertebrae CT scans ($n = 8$, mean age 62 ± 8.2 years) that was not included in the deep learning training stage was randomly selected from the local Picture Archiving and Communication Systems (PACS) database as the testing dataset for the segmentation performance evaluation.

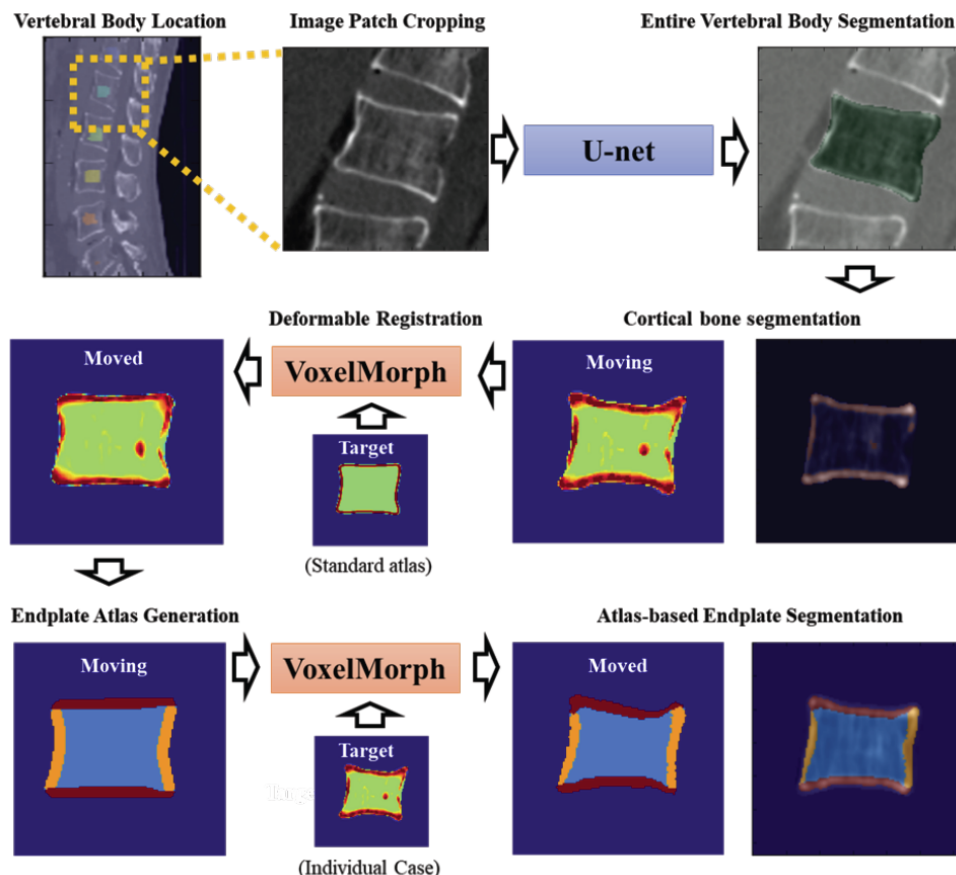


Figure 3: Illustration of the atlas-based segmentation workflow.

2.6.2. Quality of Deformable Vertebral Body Registration

Following a similar study from Valentinitich *et al.* [22], an Assessing Quality Using Image Registration Circuits (AQUIRC) [23] was used for registration quality assessment. In brief, a circuit validation of the non-rigid registration was performed. The circuit registered image would be compared to the original image to assess the registration quality. In this study, the average MSE and the Dice Coefficient were used to analyze the registration quality. Following the previously reported study [23], to calculate the registration quality in the 'circuit,' a group of at least 10 circuits formed by 5 randomly chosen images was solved altogether. Finally, a quality evaluation was performed for all the training samples and the average MSE and Dice scores were recorded.

2.6.3. Automatic Vertebral Subregions Segmentation Performance in MD-CT Images

The segmentation accuracy, Dice coefficients, and IoU were computed to evaluate the segmentation quality. The average and standard deviation of the indices in the datasets were recorded for statistical analysis.

2.7. Subregional BMD Measurement Feasibility Study

2.7.1. Data Selection

For the scan-rescan reproducibility and precision evaluation, patients that performed two scans within 1 month were retrospectively selected from the Picture Archiving and Communication Systems (PACS) database. Finally, 20 patients (16 women and 4 men with a mean age of 70.1 ± 4.8 years) with short-term rescan in the spine region were collected.

2.7.2. BMD Measurement

The BMD in each subregion of interest was measured separately. For the BMD calibration, an asynchronous BMD calibration was performed [24]. In brief, the correlation between CT value and HA-equivalent BMD value was retrospectively measured using 4 QCT datasets that were scanned with the BMD phantom (Syngo Osteo, Siemens, Germany) using the routine-CT scanning protocol. The calibration equation was determined by the linear correlation equation between the measured CT value of the BMD phantom and the known hydroxyapatite calcium (HA-Ca) equivalent density of the phantom insert.

2.7.3. Measurement Reproducibility Evaluation

The CT image datasets for the patients who underwent two abdominal CT scans were paired. The subregional BMD measurement was performed for the same vertebral segmental level in two scans. The correlation between the two scans was analyzed using the *Pearson* correlation analysis. The differences between the biomarkers measured in two repeated scans were analyzed by Bland-Altman analysis [25]. The mean of the pairwise differences was reported as bias with 95% limits of agreement. The intraclass correlation coefficient was calculated to evaluate the measurement reliability, where the ICC value closer to 1 represents the better measurement reliability.

2.8. Statistical Analysis

The statistical outcomes were reported as $\bar{x} \pm SD$. All statistical analysis was performed with MedCalc Statistical Software version 19.1 (MedCalc Software bv, Ostend, Belgium). The statistical significance was defined as $P < 0.05$.

3. RESULTS

3.1. Quality of Deformable Registration

The quality of deformable registration was evaluated by AQUIRC-MSE and Dice score in Table 1. For the segmentation mask and the registration, the AQUIRC-MSE is 0.15 ± 0.055 , and the AQUIRC-DICE coefficient is 0.98 ± 0.0059 .

Table 1: Deformable Registration Quality

Image Type	AQUIRC-MSE	AQUIRC-DICE
Segmentation Mask	0.15 ± 0.055	0.98 ± 0.0059

3.2. Automatic Segmentation Performance

The iterative U-net model showed high accuracy (0.98 ± 0.022), Dice coefficient (0.92 ± 0.062) and IoU value (0.87 ± 0.092) for the entire vertebral body segmentation. The multi-scale Otsu threshold-based cortical bone segmentation method showed high accuracy (0.95 ± 0.018), Dice coefficient (0.92 ± 0.033), and IoU value (0.85 ± 0.051). For the automatic endplate segmentation method, the segmentation performance showed high segmentation accuracy (0.89 ± 0.046) and the Dice coefficient (0.75 ± 0.09), while a moderately satisfying level of IoU value (0.61 ± 0.12) was found (Table 2).

Table 2: Cortical Bone Segmentation Accuracy using Different Threshold Technique

	Vertebral Body	Cortical	Endplates
Acc	0.98 ± 0.022	0.95 ± 0.02	0.89 ± 0.05
Dice Co.	0.92 ± 0.062	0.92 ± 0.03	0.75 ± 0.09
IoU	0.87 ± 0.092	0.85 ± 0.05	0.61 ± 0.12

(Dice Co.: Dice coefficient, IoU: Intersection over Union).

3.3. Reproducibility and Precision of Automatic Subregional BMD Measurements

In two scans, the BMD measurement of the entire vertebral body, cortical bone region, and cancellous bone region showed strong linear correlations ($r = 0.96$ for the entire region, $r = 0.95$ for the cortical region, and $r = 0.89$ for the cancellous region, respectively) with a narrow limit of agreement ($-20.4 \sim 17.9 \text{ mg/cm}^3$ for the entire region, $-39.5 \sim 33.3 \text{ mg/cm}^3$ for the cortical

region, and $-23.4 \sim 20.9 \text{ mg/cm}^3$ for the cancellous region, respectively). The measurement of the superior endplate region BMD showed a good linear correlation between two scans ($r = 0.82$) and the limits of agreement were relatively wide ($-44.9 \sim 58.9 \text{ mg/cm}^3$). However, the BMD measurement of the inferior endplate region showed a moderate linear correlation between two scans ($r = 0.63$) with wide limits of agreement ($-81.6 \sim 106.5 \text{ mg/cm}^3$) (Figure 4 and Figure 5).

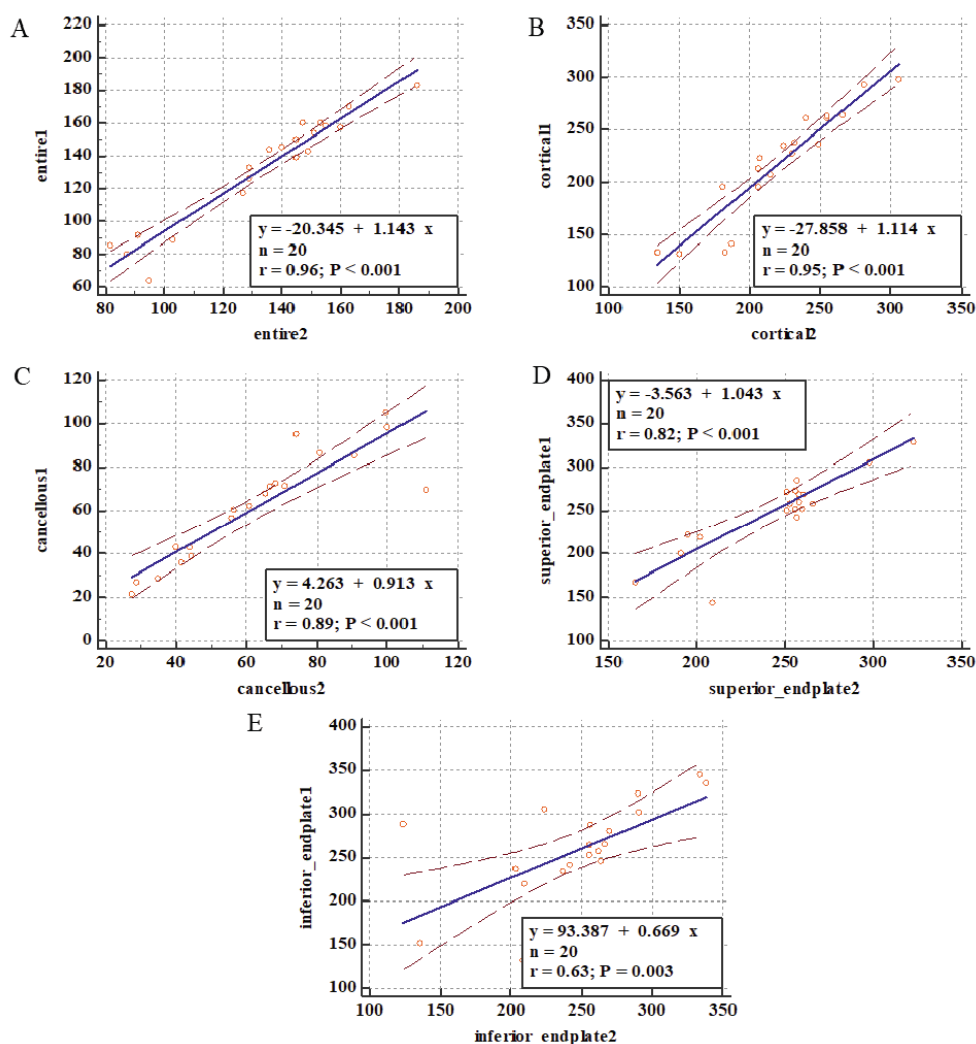


Figure 4: The linear correlation of the subregional BMD measurements between repeated scans. (A. Entire vertebral body region, B. Cortical bone region, C. Cancellous bone region, D. Superior endplate region, E. Inferior endplate region.)

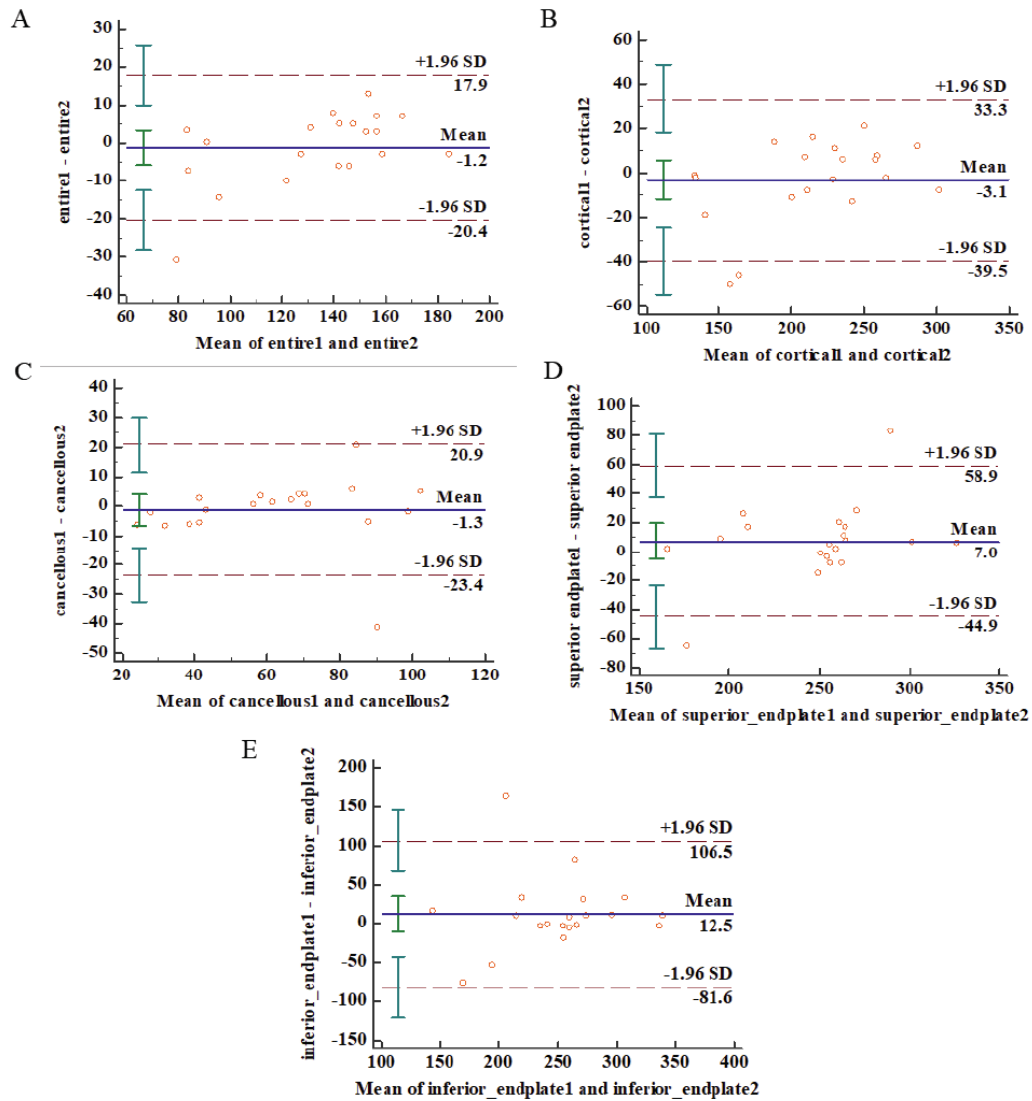


Figure 5: The Bland-Altman plot of the subregional BMD measurements between repeated scans. (A. Entire vertebral body region, B. Cortical bone region, C. Cancellous bone region, D. Superior endplate region, E. Inferior endplate region).

Between two repeated scans, the ICC was above 0.95 for the entire vertebral body, cortical region, and cancellous region BMD measurements, indicating good reliability of the repeat measurements. However, the BMD measurement in superior and inferior endplate regions showed low repeat measurement reliability with ICC < 0.9 (Table 3).

4. DISCUSSION

4.1. Automatic Vertebral Body Segmentation

Methods for semi-automatic vertebral body segmentation have been investigated for decades. One of the most used interactive methods for object segmentation is the region’s growing-based method.

Table 3: The Intraclass Correlation Coefficient of the Subregional BMD Measurements

	Entire	Cortical	Cancellous	Superior Endplate	Inferior Endplate
ICC	0.97	0.96	0.95	0.89	0.77
95% CI	0.93~0.99	0.92~0.99	0.87~0.98	0.72~0.96	0.42~0.91

(ICC: Intraclass correlation coefficient; 95% CI: 95% Confidence Interval).

Many modified methods [26] were developed for medical image segmentation based on this concept. More recently, the Grow-cut method [15] was introduced for medical imaging segmentation as a fast-semi-automatic method. The grow-cut algorithm is a competitive region growing method that can segment the image into multi-labels with high accuracy. It was validated in the vertebral body segmentation task with high accuracy and flexibility [27]. In this study, we preferred to use the Grow-cut method for semi-automatic vertebral body segmentation as it has been well studied and implemented in off-the-shelf software such as the Slicer and Photoshop for direct application.

On the other hand, the fully automatic segmentation task is more complicated and has more challenges. Vertebral body segmentation has been investigated in hundreds of studies. Due to the growth of interest in the machine learning approach in recent years, we reviewed the automatic method in two sub-fields: the non-learning-based and learning-based approach.

For the non-learning-based approach, the feature detection was usually based on basic image eigenvalues such as the Hough transformation [28], or other morphological and geometric shapes [29] that could be easily detected from images. Since the feature extraction was based on basic eigenvalues, the direct correlation between the features and the vertebral body was unclear. Thus, the workflow should be dedicatedly designed by researchers for the automatic vertebral body segmentation purpose, as the accuracy of these methods relies highly on how robust the workflows are designed.

As for the learning-based approach, the machine learning-based models have recently been widely studied as an end-to-end solution. Among all the solutions, the 3D U-net [30] still seems to be the best architecture for medical image segmentation tasks and accumulating solutions have been developed based on the basic 3D U-net architecture. However, currently, none of the fully automatic vertebral body segmentation methods have been used in a clinical study nor in clinical practice.

In this study, the hand-crafted methods were preferred as it is a 'white-box' approach with easily controlled error and effects. The methods we adopted included the classical method of multi-scale thresholding which is used widely in image processing and has been validated as a reliable method for CT image analysis [27].

4.2. Vertebral Subregions Segmentation

The vertebral bone can be further separated into the vertebral arch and vertebral body. The vertebral body further includes the endplates, cortical shell, and cancellous bone based on its sub-anatomical characters. Since the sub-anatomical parts of the vertebral body have different biophysical functions, a different part of the vertebral structure has shown its role in different spine diseases. Segmentation of the sub-structure of the vertebral body is of great importance for disease quantification. However, on the contrary to the overwhelming amount of methods dealing with whole vertebral body segmentation, there are fewer studies reported on sub-anatomical vertebral body structure segmentation.

Segmentation of the cortical and cancellous bone is one of the hard tasks for bone analysis. At the current stage, the most popular solutions are addressed to the rule-based methods. One of the widely used ideas is based on threshold segmentation. The semi-automatic threshold segmentation has been well accepted among off-the-shelf medical imaging software. Recently, a dual threshold-based method was proposed for micro-CT cortical and cancellous bone segmentation [31]. Another research orientation is to establish mathematical models to decompose the signal of cortical and cancellous bone [32]. Although the mathematical modeling method achieved higher accuracy on the 'real' cortical bone segmentation compared to the HR-CT gold standard outcome, the modeling function is varied in different CT scanners and cannot be directly used without adjustment for each type of CT scanner. More recently, the histogram clustering threshold method is one of the new ideas for bone segmentation [33]. The basic concept is that the cortical and cancellous bone has a different signal range that forms the different parts of the histogram. For a high-resolution CT, the histogram can be clustered by a threshold and then used for cortical bone and cancellous bone separation. In this study, the histogram clustering method was further researched since it is a global analysis approach that can be easily implemented without prior knowledge of 3D bone geometry and mathematical modeling functions.

Even though the cortical bone segmentation methods have been relatively well studied by researchers, to our knowledge, only one study that dealt with the endplate segmentation task was reported at the present day [10]. However, that study was developed for mice bone image studies in micro-CT.

The manifestations of the endplates in micro-CT images are far different from the clinical CT. To date, the automatic method that applies to vertebral endplate segmentation in clinical CT images has been rarely reported. In this study, a hybrid method combining the learning-based segmentation and atlas-based deformable segmentation was proposed to achieve automatic endplate segmentation and achieved a good performance on the validation datasets.

5. CONCLUSION

Through this study, we found the deep learning-based approach to be practical and efficient for vertebral subregional BMD analysis. The validation experiments further verified that the automatic approach can achieve high segmentation accuracy and BMD measurement precision for vertebral cortical and cancellous bone regions. This study provides evidence that the automatic approach has the potential capacity to be a practical tool for vertebral subregional osteoporosis analysis.

ACKNOWLEDGEMENT

This work was supported by the Shenzhen Significant Strategy Layout Project (JCYJ 20170413162104773) for Prof. William W. Lu; and the Science, Technology, and Innovation Commission of Shenzhen Municipality (JCYJ 20180306173518936) for Dr. Feng Zhu.

REFERENCES

- [1] Gallardo-Estrella L, *et al.*, Normalizing computed tomography data reconstructed with different filter kernels: effect on emphysema quantification. *Eur Radiol*, 2016; 26(2): 478-86. <https://doi.org/10.1007/s00330-015-3824-y>
- [2] Smith AD. Screening of Bone Density at CT: An Overlooked Opportunity. *Radiology*, 2019; 291(2): 368-369. <https://doi.org/10.1148/radiol.2019190434>
- [3] Engelke K, *et al.*, Reanalysis precision of 3D quantitative computed tomography (QCT) of the spine. *Bone*, 2009; 44(4): 566-72. <https://doi.org/10.1016/j.bone.2008.11.008>
- [4] Yao J, *et al.*, A multi-center milestone study of clinical vertebral CT segmentation. *Comput Med Imaging Graph*, 2016; 49: 16-28. <https://doi.org/10.1016/j.compmedimag.2015.12.006>
- [5] McKay M, *et al.*, Association of vertebral endplate microstructure with bone strength in men and women. *Bone*, 2020; 131: 115147. <https://doi.org/10.1016/j.bone.2019.115147>
- [6] Cody DD, *et al.*, Correlations between vertebral regional bone mineral density (rBMD) and whole bone fracture load. *Spine (Phila Pa 1976)*, 1991; 16(2): 146-54. <https://doi.org/10.1097/00007632-199116020-00009>
- [7] Che-Nordin N, *et al.*, Prevalent osteoporotic vertebral fractures more likely involve the upper endplate than the lower endplate and even more so in males. *Ann Transl Med*, 2018; 6(22): 442. <https://doi.org/10.21037/atm.2018.10.61>
- [8] Palepu V, Rayaprolu SD and Nagaraja S. Differences in Trabecular Bone, Cortical Shell, and Endplate Microstructure Across the Lumbar Spine. *Int J Spine Surg*, 2019; 13(4): 361-370. <https://doi.org/10.14444/6049>
- [9] Vaananen SP, *et al.*, Automated segmentation of cortical and trabecular bone to generate finite element models for femoral bone mechanics. *Med Eng Phys*, 2019; 70: 19-28. <https://doi.org/10.1016/j.medengphy.2019.06.015>
- [10] Shi-Jian Liu ZZ, Jeng-Shyang Pan, Sheng-Hui Liao, Mice endplate segmentation from micro-CT data through graph-based trabecula recognition. 2019. <https://doi.org/10.1186/s13640-019-0456-1>
- [11] Falcinelli C, *et al.*, Can CT image deblurring improve finite element predictions at the proximal femur? *J Mech Behav Biomed Mater*, 2016; 63: 337-351. <https://doi.org/10.1016/j.jmbbm.2016.07.004>
- [12] Pakdel A, *et al.*, Restoration of Thickness, Density, and Volume for Highly Blurred Thin Cortical Bones in Clinical CT Images. *Ann Biomed Eng*, 2016; 44(11): 3359-3371. <https://doi.org/10.1007/s10439-016-1654-y>
- [13] Museyko O, Gerner B and Engelke K. A new method to determine cortical bone thickness in CT images using a hybrid approach of parametric profile representation and local adaptive thresholds: Accuracy results. *PLoS One*, 2017; 12(11): e0187097. <https://doi.org/10.1371/journal.pone.0187097>
- [14] Treece GM and Gee AH. Independent measurement of femoral cortical thickness and cortical bone density using clinical CT. *Med Image Anal*, 2015; 20(1): 249-64. <https://doi.org/10.1016/j.media.2014.11.012>
- [15] Vezhnevets V. "GrowCut" - Interactive Multi-Label N-D Image Segmentation By Cellular Automata. 2004.
- [16] Elhabian SY, *et al.*, Shape Works Studio: Particle-based Shape Correspondence and Visualization Software, in Technical Report. 2017, Scientific Computing and Imaging Institute, University of Utah.
- [17] Lessmann N, *et al.*, Iterative fully convolutional neural networks for automatic vertebra segmentation and identification. *Med Image Anal*, 2019; 53: 142-155. <https://doi.org/10.1016/j.media.2019.02.005>
- [18] Feng Y, *et al.*, A multi-scale 3D Otsu thresholding algorithm for medical image segmentation. *Digital Signal Processing*, 2017; 60: 186-199. <https://doi.org/10.1016/j.dsp.2016.08.003>
- [19] Marstal K, *et al.* Simple Elastix: A User-Friendly, Multi-lingual Library for Medical Image Registration. in 2016 IEEE Conference on Computer Vision and Pattern Recognition Workshops (CVPRW). 2016. <https://doi.org/10.1109/CVPRW.2016.78>
- [20] Balakrishnan G, *et al.*, Voxel Morph: A Learning Framework for Deformable Medical Image Registration. *IEEE Trans Med Imaging*, 2019. <https://doi.org/10.1109/TMI.2019.2897538>
- [21] Salehi SSM, Gholipour ED A, Tversky Loss Function for Image Segmentation Using 3D Fully Convolutional Deep Networks, in Machine Learning in Medical Imaging. MLMI 2017. Lecture Notes in Computer Science, SY. Wang Q, Suk HI, Suzuki K, Editor. 2017; Springer, Cham. 379-387. https://doi.org/10.1007/978-3-319-67389-9_44
- [22] Valentinitich A, *et al.*, Regional analysis of age-related local bone loss in the spine of a healthy population using 3D voxel-based modeling. *Bone*, 2017; 103: 233-240. <https://doi.org/10.1016/j.bone.2017.06.013>
- [23] Datteri R, *et al.*, Applying the algorithm "assessing quality using image registration circuits" (AQUIRC) to multi-atlas segmentation 2014; 9034: 90341F. <https://doi.org/10.1117/12.2043756>

- [24] Budoff MJ, *et al.*, Measurement of phantomless thoracic bone mineral density on coronary artery calcium CT scans acquired with various CT scanner models. *Radiology* 2013; 267(3): 830-6.
<https://doi.org/10.1148/radiol.13111987>
- [25] Bland JM and Altman DG. Statistical methods for assessing agreement between two methods of clinical measurement. *Lancet* 1986; 1(8476): 307-10.
[https://doi.org/10.1016/S0140-6736\(86\)90837-8](https://doi.org/10.1016/S0140-6736(86)90837-8)
- [26] Heimann T. New methods for leak detection and contour correction in seeded region growing segmentation. 2004.
- [27] Egger J, Nimsy C and Chen X. Vertebral body segmentation with GrowCut: Initial experience, workflow and practical application. *SAGE Open Med* 2017; 5: p. 2050312117740984.
<https://doi.org/10.1177/2050312117740984>
- [28] Baum T, *et al.*, Automatic detection of osteoporotic vertebral fractures in routine thoracic and abdominal MDCT. *Eur Radiol*, 2014; 24(4): 872-80.
<https://doi.org/10.1007/s00330-013-3089-2>
- [29] Mastmeyer A, *et al.*, A hierarchical 3D segmentation method and the definition of vertebral body coordinate systems for QCT of the lumbar spine. *Med Image Anal* 2006; 10(4): 560-77.
<https://doi.org/10.1016/j.media.2006.05.005>
- [30] Çiçek Ö, *et al.*, 3D U-Net: learning dense volumetric segmentation from sparse annotation. *International conference on medical image computing and computer-assisted intervention*, 2016; (pp. 424-432).
https://doi.org/10.1007/978-3-319-46723-8_49
- [31] Buie HR, *et al.*, Automatic segmentation of cortical and trabecular compartments based on a dual threshold technique for in vivo micro-CT bone analysis. *Bone* 2007; 41(4): 505-15.
<https://doi.org/10.1016/j.bone.2007.07.007>
- [32] Pearson RA and GM. Treece, Measurement of the bone endocortical region using clinical CT. *Med Image Anal*, 2018. 44: p. 28-40.
<https://doi.org/10.1016/j.media.2017.11.006>
- [33] Indraswari R. Automatic Segmentation of Mandibular Cortical Bone on Cone-Beam CT Images Based on Histogram Thresholding and Polynomial Fitting 2019.
<https://doi.org/10.22266/ijies2019.0831.13>

Received on 16-09-2020

Accepted on 22-10-2020

Published on 09-11-2020

DOI: <http://dx.doi.org/10.12974/2313-0954.2020.07.1>

© 2020 Chentian Li *et al.*; Licensee Savvy Science Publisher.

This is an open access article licensed under the terms of the Creative Commons Attribution Non-Commercial License (<http://creativecommons.org/licenses/by-nc/3.0/>) which permits unrestricted, non-commercial use, distribution and reproduction in any medium, provided the work is properly cited.